THE PINHOLE INTERFACE FOR IMS/MS

Glenn E. Spangler[1]

Environmental Technologies Group, Inc., 1400 Taylor Avenue, Baltimore, MD 21204-9840

ABSTRACT

An important supplementary technique for ion mobility spectrometry (IMS) is mass spectrometry (MS). A mass spectrometer coupled to an ion mobility spectrometer (IMS/MS) can provide significant information on the composition of the ions contributing to an ion mobility peak. On the other hand, the interpretation of IMS/MS results requires knowledge of processes which can occur at the pinhole interface. When the ion composition is a mixture of ion clusters, the observed cluster distribution may not be an accurate representation of the ion clusters in the IMS. Depending on the buffer gas, lower clusters can form by equilibrating with reduced concentrations in the continuum regime of the expansion and larger clusters can form by collisional stabilization in the cooled jet stream. Besides water, nitrogen molecules can also add to the ion clusters. Even though nitrogen is non-polar, this addition is made possible by an ion-induced dipole interaction between the ion and molecule.

INTRODUCTION

A favorite activity in ion mobility spectrometry (IMS) is to correlate ion mobility with the molecular weight and structure of ions.[1,2,3] The motivation behind these activities is that the mobility of an ion colliding with a gas is inversely proportional to the ion's reduced mass and collision cross section.[4,5] While many interesting observations have been made on ion structures using this approach,[6,7,8,9,10,11] one cannot be assured that the ions formed in IMS are bare ions. Rather the ions are often clusters containing neutral molecules other than the analyte.[12] Mass spectrometry is invaluable in identifying the composition of these ion clusters.

An IMS/MS is a IMS coupled to a mass spectrometer in such a way to allow sampling of the ions formed in the IMS by the MS. This is accomplished by providing a hole in the collector plate of the IMS and passing the ions through a pinhole interface into the vacuum system containing the mass spectrometer. Immediately behind the pinhole are focussing lenses which focus the ions unto the entrance aperture of the mass spectrometer. The pinhole interface is very similar to jet samplers used to sample ions in atmospheric pressure ionization mass spectrometry.[13,14] While the pinhole is very efficient in transmitting ions into the vacuum system, it also has a tendency to distort ion distributions. Since ion mobilities in IMS are dependent upon ion cluster distributions, this tendency interferes with the original purpose for collecting IMS/MS data.[15] Without knowledge of the processes leading to the distortion, absolute certainty concerning ion composition is lacking. Although the difficulty has not gone unnoticed in the open literature, approaches to IMS research have not been addressed.

Because the mean free path for an ion at 1 atmosphere is three orders of magnitude less than the diameter of a typical pinhole (20 - 50 micrometers), there will be many collisions between the molecules (and ions) as they enter the vacuum system of an IMS/MS. The current theory for the gas flow through a pinhole is isentropic free-jet expansion.[16,17,18,19] In the jet, the density of the gas decreases monotonically and the enthalpy of the source gas is converted into directed flow.[20] According to Miller, the fluid mechanical structure of a jet is dependent not only on hydrodynamic parameters (e.g., stagnant pressure, initial temperature, orifice area, etc.), but also the

---

[1]Current Address: 1209 Malbay Drive, Lutherville, MD 21093

length scale of the apparatus into which the jet is expanding.[21] For an unconstrained jet, the flow becomes supersonic and the expansion is surrounded by a concentric barrel shock terminated by a perpendicular shock known as the Mach disc.[22] This shock structure protects the expansion region from collisions with the background gas and the degree of ionization remains frozen to that of the source.[22] On the other hand when Searcy and Fenn used a 100 micron pinhole diameter to sample a 4.6 torr partial pressure of water, they noticed a sampling error which was dependent on stagnant pressure and buffer gas composition.[23,24,25] Ion clusters were formed which tended towards supersaturation. When Zook and Grimsrud reduced the pinhole diameter to 25 microns, the cluster distribution was dependent upon source temperature (125-250 °C) and could be accurately determined using a helium or hydrogen buffer gas.[26]

This paper describes experiments conducted to characterize the sampling capabilities of a pinhole interface between an IMS and an MS. When performing studies of this type, it is necessary to eliminate collisional dissociation mechanisms. Collisionally induced dissociation (i.e., "cluster buster") is often used to simplify mass spectra obtained from an atmospheric pressure ionization source.[27,28,29] This is accomplished by exposing the ion clusters to an elevated potential drop as they enter the vacuum region. While this may be a good way to prepare an ion sample for subsequent mass analysis, the conditions of the ionization source are forgotten in the process. This issue will be addressed.

EXPERIMENTAL METHODS

The investigations were conducted using an IMS/MS previously described in the open literature.[30] Improvements to the system included replacing the stacked-ring IMS cell with an all-ceramic IMS cell, upgrading the quadrupole mass spectrometer to an EXTREL C50 quadrupole mass spectrometer,[31] and installing a turbomolecular pump in place of the 4-inch diffusion pump. These are shown in Figure 1.

Structurally, the IMS cell contained three main parts:

a. Reactor (approx. 2 cm long, 2.5 cm internal diameter, 1.16 megohm resistance)

b. Drift tube (11.4 cm long, 3.8 cm internal diameter, 11.08 megohm resistance)

c. Membrane inlet (OV-101 impregnated microporous Teflon membrane, 1.3 cm^2 area).[32]

The ionization source was a cylindrical ring of ^{63}Ni foil approximately one inch in diameter and one centimeter long.[33] Although the IMS cell contained a shutter grid between the reactor and drift tube, it was biased open during the experiments so that it continuously conducted ion current. Since the ion current was measured using the electronics of the mass spectrometer, the IMS cell contained no ion collector. The temperature was measured using four thermocouples placed in contact with the pinhole mounted on the vacuum flange leading into the mass spectrometer, around the drift tube of the IMS halfway between the shutter grid and the mass spectrometer, and in contact with the reactor and membrane inlet of the IMS. Using strategically located heater tapes, the temperature at these four locations were continuously monitored and automatically controlled using temperature controllers. Thermal gradients were minimized by preheating the carrier and drift gases before they entered the cell.

Purified air or argon (Matheson UN 1006)[34] was used for the carrier, drift and sample gases of the cell. The purified air was generated using a Balston CO_2 remover.[35] Before being introduced into the cell, both gases were passed through activated 13X molecular sieve scrubbers.[36] The 13X molecular sieve scrubbers were activated with a purging flow of prepurified nitrogen at 300 °C for 24 hours before each experiment. The water content of the gases was monitored using a DuPont 703 phosphorous pentoxide hygrometer.[37] Typically the purified air contained 0.1 to 1.5 ppm water and the argon contained 1.5 to 1.6 ppm water. The water content

increased within these ranges as the scrubbers aged. Since the drift gas flowed between the vacuum flange of the mass spectrometer and the mounting flange for the IMS, it also served as a curtain gas for the pinhole. After flowing through the membrane inlet, the carrier gas entered the IMS cell near the shutter grid and exhausted with the drift gas through the reactor (i.e., unidirectional flow).

Since this paper is about processes that occur at the pinhole, this part of the IMS/MS is very important. An expanded sketch is shown in Figure 2. The ion sampling pinhole was mounted at the apex of a conical extension to the vacuum flange leading into the mass spectrometer. The angle for the cone was 50° with a height of 2.2 cm. These dimensions placed the pinhole 4.18 cm from the focussing lens assembly of the mass spectrometer. Immediately behind the pinhole was a 2.45 cm diameter by 2.27 cm long wire basket. This wire basket was mechanically and electrically attached to the first ion focussing lens and served to focus the ions entering the mass spectrometer onto the lens assembly. The wire basket also allowed gas entering the pinhole to freely expand into the vacuum system. With a bubble flowmeter, the volumetric flow of air passing through the pinhole was measured as 5.3 cc(RTP)/min. For the rated 450 L/s pumping speed for the turbomolecular pump behind the pinhole, this air flow corresponds to a baseline pressure of 1.5×10^{-4} Torr in the inlet chamber (i.e., the chamber that contained the focussing lenses). The actual pressure was 1.8×10^{-4} Torr as indicated by a vacuum gauge attached to the pumping line. When averaged across the area of the pinhole, the measured air flow corresponds to a linear air velocity of 179.3 m/s (<350 m/s, the velocity of sound in dry air).

The remainder of the operating conditions for the mass spectrometer are shown in Table 1.

RESULTS

Figures 3 and 4 show the positive and negative reactant ions generated in purified air using two potential distributions for the ion focussing lenses. The two potential distributions are given in Table 1 and were selected in an effort to influence the energy of the ions as they entered the vacuum system. The water content of the purified air was 1.5 ppm. The major positive ions were $H^+(H_2O)_n(N_2)_m$ with masses 55, 73, 83, 91, 101, 111, 129, 139 and 157 corresponding to n = 3 to 5 and m = 0 to 3. The major negative ions were $O_2^-(H_2O)_n(N_2)_m$ with masses 32, 50, 68, 78, 86, 96 and 124 corresponding to n = 0 to 3 and m = 0 to 2. Also the negative ions with masses 82, 100, 110, 118 and 138 are due to $O_4^-(H_2O)_n(N_2)_m$ with n = 1 to 4 and m = 0 to 2. All these ions are clusters involving water and nitrogen adducts.

A problem with these ion assignments is that the mass 28 difference assigned to nitrogen could also be carbon dioxide. Nitrogen has a zero dipole moment while carbon monoxide has a 0.10×10^{-18} e.s.u. dipole moment.[38] Although carbon monoxide was not added intentionally to the present experiments and nitrogen was a major component of the carrier and drift gases, it cannot be argued that carbon monoxide was not present as a trace contaminant during the experiments. This issue will be addressed when the data of Figure 5 are discussed.

The amplitude ratios between neighboring clusters are shown in Table 2. These amplitude ratios are proportional to the equilibrium constant for

$$I^+ + S \rightleftharpoons I^+(S)$$
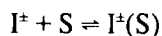
where I^+ is the ion and S is the solvating molecule. Except for the large unexplained discrepancy for the $O_2^- + H_2O \rightleftharpoons O_2^-(H_2O)$ reaction, the data for the two of lens potential distributions are in basic agreement. These results demonstrate that the potential distribution on the focussing lenses does not cause the clusters to dissociate as they enter the vacuum region.[28,29] Considering the fact that the potential applied to lens #1 located immediately behind the pinhole was increased an order of magnitude, a considerable margin of safety is indicated. Because there was nearly an order of magnitude more ion signal when the higher lens potentials were used, the remainder

117

TABLE 1: Operating Parameters for the IMS/MS

PARAMETER		VALUE
Pressures	Mass Spectrometer Focussing Lenses	2.6×10^{-6} Torr 1.8×10^{-4} Torr
Voltages	Reaction Region Hi Drift Region Hi Aperture Grid Pinhole Focussing Lens #1 Focussing Lens #2 Focussing Lens #3 Focussing Lens #4 Focussing Lens #5 Pole Zero	$\pm$ 2471 Volts ($\pm$ 1549 Volts w Argon) $\pm$ 1922 Volts ($\pm$ 1000 Volts w Argon) $\pm$ 129 Volts ($\pm$ 67 Volts w Argon) Ground $\mp$ 44.3 Volts or $\mp$ 4.7 Volts $\mp$ 17.5 Volts or $\mp$ 1.2 Volts $\mp$ 80.2 Volts or $\mp$ 20.1 Volts $\mp$ 30.4 Volts or $\mp$ 17.9 Volts $\mp$ 45.0 Volts or $\mp$ 14.8 Volts $\mp$ 8.5 to $\pm$ 1.5 Volts, or $\mp$ 21 to $\mp$ 11 Volts
Temperatures	Membrane Inlet Reaction Region Drift Region Pinhole Mass Spectrometer	48 °C 45 °C 54 °C 53 °C Unheated
Gas Flows	Carrier Gas Drift Gas Sample Gas	210 cc/min 336 cc/min 240 cc/min

of the data in this report were collected using that potential distribution. This means that lens #1 was biased at $\pm$ 44.3 Volts and the quadrupole mass analyzer was near ground potential.

Figure 5 compares positive ion spectra when purified air was used for the carrier, drift and sample gases; when argon was used for the carrier, drift and sample gases; and when purified air was used for the carrier and sample gases and argon was used for the drift gas. These data show that the ions with masses 101, 129 and 157 previously attributed to nitrogen adducts were observed only when purified air was used for the carrier and sample gases. They were not observed when argon was used for all the gases. When argon was used for the carrier gas, ions with mass 55, 73, 95, 113, 135 and 153 were observed which can be assigned the structures $H^+(H_2O)_n(Ar)_m$ with n = 3 and 4 and m = 0 to 2. It is clear from this result that the nitrogen adducts are formed in the reactor and that the nitrogen adducts are not CO adducts. Because CO has a dipole moment greater than argon, CO adducts should have been observed in the presence of the argon carrier gas.

Recorded in Table 3 are the amplitude ratios observed when purified air, and then argon, were used for the drift gas. While several of the ratios are larger for argon to indicate that larger clusters are formed in argon, this result may be due to differences in water content between the two gases. Experiments were not run with a known concentration of water introduced in both gases. While Zook and Grimsrud report extensive cluster

Table 2: Amplitude Ratio Between Various Reactant Ion Clusters

Positive Reactant Ions			Negative Reactant Ions		
Reaction	Lens Potentials		Reaction	Lens Potentials	
	High	Low		High	Low
$H^+(H_2O)_3 \rightleftharpoons H^+(H_2O)_4$	4.9	4.3	$O_2^- \rightleftharpoons O_2^-(H_2O)$	21	4.9
$H^+(H_2O)_4 \rightleftharpoons H^+(H_2O)_5$	0.06	0.09	$O_2^-(H_2O) \rightleftharpoons O_2^-(H_2O)_2$	1.6	1.9
$H^+(H_2O)_3 \rightleftharpoons H^+(H_2O)_3(N_2)$	0.69	0.78	$O_2^-(H_2O)_2 \rightleftharpoons O_2^-(H_2O)_3$	0.07	0.07
$H^+(H_2O)_3(N_2) \rightleftharpoons H^+(H_2O)_3(N_2)_2$	0.81	0.48	$O_2^-(H_2O) \rightleftharpoons O_2^-(H_2O)(N_2)$	0.29	0.34
$H^+(H_2O)_3(N_2)_2 \rightleftharpoons H^+(H_2O)_3(N_2)_3$	0.66	0.73	$O_2^-(H_2O)_2 \rightleftharpoons O_2^-(H_2O)_2(N_2)$	0.15	0.15
$H^+(H_2O)_4 \rightleftharpoons H^+(H_2O)_4(N_2)$	0.47	0.43	$O_2^-(H_2O)_2(N_2) \rightleftharpoons O_2^-(H_2O)_2(N_2)_2$	0.19	0.21
$H^+(H_2O)_4(N_2) \rightleftharpoons H^+(H_2O)_4(N_2)_2$	0.38	0.32	$O_4^- \rightleftharpoons O_4^-(H_2O)$	5.45	7.29
$H^+(H_2O)_4(N_2)_2 \rightleftharpoons H^+(H_2O)_4(N_2)_3$	0.20	0.21	$O_4^-(H_2O) \rightleftharpoons O_4^-(H_2O)_2$	0.71	0.82
			$O_4^-(H_2O)_2 \rightleftharpoons O_4^-(H_2O)_3$	0.07	0.05
			$O_4^-(H_2O) \rightleftharpoons O_4^-(H_2O)(N_2)$	0.37	0.43
			$O_4^-(H_2O)(N_2) \rightleftharpoons O_4^-(H_2O)(N_2)_2$	0.31	0.32

growth when analyzing higher water concentrations using an argon buffer gas, the current data cannot be used to either confirm or deny their results.[26] Certainly, Amirav et al. report that cooling increases in the order of Xe > Kr > Ar > Ne > He for jet expansions, a trend reflected in Zook and Grimsrud's data..[39]

Finally, the carrier gas flow was removed from the IMS cell and purified air was used for the drift gas. Since the drift gas exhausted through the reactor of the cell, the IMS cell was being totally purged with purified air. Next, the 13X scrubber in line with the purified air was reactivated and all fittings checked for leak tightness. When this was completed, the cell exhaust was drier than could be reliably measured with the hygrometer. Using estimation procedures described in the hygrometer manual, the water content of the exhausting air was probably on the order of 100 ppb. The positive and negative reactant ions collected for this condition are shown in Figure 6.

Immediately after the data of Figure 6 were collected, a 5 mm bore by 7.5 cm long diffusion tube of deionized water was placed in line with the drift gas line of the cell. This caused the water content of the gas exhausting from the cell to increase to 13.1 ppm. This hygrometer reading agreed with gravimetric measurements performed on the diffusion tube which indicated 12.0 to 13.4 ppm water was being added to the drift gas. When the water concentration stabilized, the IMS signatures of Figure 7 were collected. The effects of the increased water concentration were immediately obvious. In the positive ion mode, the amplitude ratio for the $H^+(H_2O)_4/H^+(H_2O)_3$ ions increased from 0.9 to 8.1 and in the negative ion mode, the amplitude ratio for the $O_2^-(H_2O)_2/O_2^-(H_2O)$ ions increased from 0.16 to 3.1. These amplitude ratios are shown in Table 4.

Table 3: Amplitude Ratios for Reactant Ion Clusters Using Two Drift Gases

Reaction	P.A. Drift Gas	Ar Drift Gas	Reaction	P.A. Drift Gas	Ar Drift Gas
$H^+(H_2O)_3 \rightleftharpoons H^+(H_2O)_4$	1.5	3.2	$O_2^- \rightleftharpoons O_2^-(H_2O)$	18.5	15.1
$H^+(H_2O)_4 \rightleftharpoons H^+(H_2O)_5$	0.05	0.07	$O_2^-(H_2O) \rightleftharpoons O_2^-(H_2O)_2$	0.32	0.79
$H^+(H_2O)_3 \rightleftharpoons H^+(H_2O)_3(N_2)$	0.92	1.0	$O_2^-(H_2O)_2 \rightleftharpoons O_2^-(H_2O)_3$	-	0.06
$H^+(H_2O)_3(N_2) \rightleftharpoons H^+(H_2O)_3(N_2)_2$	0.91	0.72	$O_2^-(H_2O) \rightleftharpoons O_2^-(H_2O)(N_2)$	0.19	0.63
$H^+(H_2O)_3(N_2)_2 \rightleftharpoons H^+(H_2O)_3(N_2)_3$	0.39	0.73	$O_2^-(H_2O)(N_2) \rightleftharpoons O_2^-(H_2O)(N_2)_2$	0.17	0.49
$H^+(H_2O)_4 \rightleftharpoons H^+(H_2O)_4(N_2)$	0.05	0.08	$O_2^-(H_2O)_2 \rightleftharpoons O_2^-(H_2O)_2(N_2)$	0.19	0.56
$H^+(H_2O)_4(N_2) \rightleftharpoons H^+(H_2O)_4(N_2)_2$	0.33	0.63	$O_4^- \rightleftharpoons O_4^-(H_2O)$	4.0	12.7
$H^+(H_2O)_4(N_2)_2 \rightleftharpoons H^+(H_2O)_4(N_2)_3$	0.24	0.26	$O_4^-(H_2O) \rightleftharpoons O_4^-(H_2O)_2$	0.12	0.55
			$O_4^-(H_2O)_2 \rightleftharpoons O_4^-(H_2O)_3$	0.12	0.54
			$O_4^-(H_2O) \rightleftharpoons O_4^-(H_2O)(N_2)$	0.30	0.50
			$O_4^-(H_2O)(N_2) \rightleftharpoons O_4^-(H_2O)(N_2)_2$	0.21	0.39

If it is assumed that the water clusters are in equilibrium and their concentrations are related to each other through previously measured thermochemical data, it is possible to estimate the water concentration in the IMS cell using the mass spectrometer data. This is done using the relationship

$$C_{H2O} = [I^+(H_2O)_{n+1}]/[I^+(H_2O)_n]\{\exp(\Delta G/RT)\}$$

where $[I^+(H_2O)_n]$ is the amplitude of the n-th ion cluster and ΔG is the free energy for

$$I^+(H_2O)_n + H_2O \rightleftharpoons I^+(H_2O)_{n+1}$$
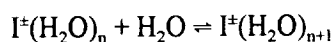
These estimates are also shown in Table 4.

Table 4 shows a large discrepancy between the calculated values and the actual value of 13 ppm. The calculated values obtained from smaller clusters underestimate the water concentration, while the calculated values obtained from larger clusters overestimate the water concentration. Efforts to adjust the values by raising or lowering the temperature or by including an extra energy term in the exponential were unsuccessful. If the thermochemical data are correct, it is apparent that the processes occurring behind the pinhole are complex and cannot be explained in terms of simple cooling or collisional dissociation.

DISCUSSION

Because it was shown that the lens potentials have little effect on ion distributions, the results of Table 4 must be

Table 4: Comparison of 13 ppm Water Concentration with Thermodynamic Values
Calculated from Peak Amplitude Ratios.*

Positive Reactant Ions			Negative Reactant Ions		
Reaction	Ampl Ratio	C_{H2O} (ppm)	Reaction	Ampl Ratio	C_{H2O} (ppm)
$H^+(H_2O)_2 + H_2O \rightleftharpoons H^+(H_2O)_3$	13	0.04	$O_2^- + H_2O \rightleftharpoons O_2^-(H_2O)$	30	0.37
$H^+(H_2O)_3 + H_2O \rightleftharpoons H^+(H_2O)_4$	8.1	54	$O_2^-(H_2O) + H_2O \rightleftharpoons O_2^-(H_2O)_2$	3.1	0.49
$H^+(H_2O)_4 + H_2O \rightleftharpoons H^+(H_2O)_5$	0.16	126	$O_2^-(H_2O)_2 + H_2O \rightleftharpoons O_2^-(H_2O)_3$	0.14	10
$H^+(H_2O)_5 + H_2O \rightleftharpoons H^+(H_2O)_6$	0.12	885			

* P. Kebarle, S.K. Searles, A. Zolla, J. Scarborough, M. Arshadi *J. Amer. Chem. Soc.* 1967, *89*, 6393; M. Arshadi, P. Kebarle *J. Phys. Chem.* 1970, *74*, 1483.

due to gas dynamics accompanying ion sampling. As mentioned in the introduction, the current accepted theory for the flow of gas through a 25 micrometer pinhole into vacuum is isentropic free-jet expansion.[40] Isentropic expansions are expansions in which the entropy remains constant and the various degrees of freedom (translation, rotation, vibration) of the gas remain in equilibrium.

Another characteristic of jet expansions is that there is a narrowing of the velocity distribution. This narrowing arises from those statistically favored molecules which have a velocity component in the direction of the expansion as they pass through the pinhole and from geometric channeling by the pinhole.[40] Accompanying the narrowing of the velocity distribution is a lowering of the temperature. As the temperature drops, so does the velocity of sound which leads to a change in conditions required to establish supersonic expansion.

For the present experiments, the linear air velocity through the pinhole was 179.3 m/s. While this velocity is significantly less than the standard velocity of sound in dry air (350 m/s), it does correspond to the velocity of sound at a reduced temperature and pressure. Assuming a square root dependence for the velocity of sound on temperature,[41] the required temperature is 26% of the standard temperature, or approximately 84 °C. To maintain isentropic conditions for the expansion, this temperature corresponds to a pressure of 26 Torr immediately behind the pinhole.

Assuming that supersonic expansion was occurring, it is possible to roughly locate the Mach disc. Theoretically, the location (x_M) is given by[42]
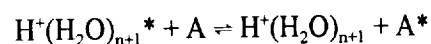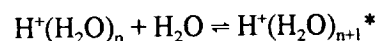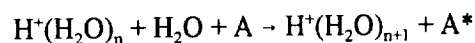
$$x_M = 0.67D[P_o/P]^{1/2}$$

where D is the pinhole diameter and P is the background pressure in the expansion chamber. Since the pinhole diameter was 25 microns and the background pressure was 1.8×10^{-4} torr, x_M was 3.4 cm. Because the distance between the pinhole and first focussing lens in the mass spectrometer was 4.2 cm, this location for the Mach disc was within the wire basket (see Figure 2) used to pull the ions towards the focussing lenses. If this is the case, then all the ions analyzed by the mass spectrometer had to pass through the Mach disc. The literature is undecided on what might happen to an ion cluster if this should occur.[22]

It turns out, however, that this may not be a problem because Miller notes that in a system were the background pressure is 10^{-4} and the stagnation pressure is atmospheric, "the continuum pressure just upstream of the Mach disc would be predicted to be $P_M \sim 10^{-9}$ torr, and the upstream mean free path about 25 cm!"[21] If this should occur, the mean free path would be greater than the 2.45 cm diameter for the wire basket, meaning the mean free path is much greater than the instrument dimension. Since shock wave thicknesses are on the order of the mean free path, it is doubtful that a Mach disc could form. For such a condition, a smooth transition from continuum to free-molecular flow would occur; the jet rays being attenuated by the background gas and surface reflected molecules in a Beer's Law like fashion. Hayes claims the expansion can be broken down into three distinct regimes: (1) continuum flow, (2) transition flow and (3) free molecular flow.[40]
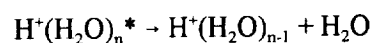
The results of Table 4 show that when the ions participate in the expansion, there are opposing tendencies for cluster growth (as evidenced by the high concentration derived from the $H^+(H_2O)_5 + H_2O \rightleftharpoons H^+(H_2O)_6$ reaction) and desolvation (as evidenced by the low concentration derived from the $H^+(H_2O)_2 + H_2O \rightleftharpoons H^+(H_2O)_3$ reaction). In their studies Zook and Grimsrud observed similar tendencies.[26] They noted that the "MS^- and M^- ion density ratios *for dimethyl sulfoxide (DMSO)* were actually somewhat less than the expected ion intensity abundance ratio, suggesting that cluster growth due to a cooling effect in the aperture was not the dominant force in perturbing the ion distribution."[26] When describing their results using methane and nitrogen buffer gases, they claimed that "two opposing processes are operative within the jet expansions for the proton hydrates. One of these causes cluster growth, as evidenced by the prominent ions of n = 8 and the other leads to smaller clusters, as evidenced by the prominent ions at n = 4."

Zook and Grimsrud tried to interpret their data in terms of Searcy's kinetic model based on Buckle's suggestions for neutral clustering.[24,43] This model assumes that all radiative transitions have long time constants compared with collision frequency, and equilibrium is maintained by the following series of reactions.

increasing n (parallel three body and energetic cluster formation reactions),

$$H^+(H_2O)_n + H_2O + A \rightarrow H^+(H_2O)_{n+1} + A^*$$

$$H^+(H_2O)_n + H_2O \rightleftharpoons H^+(H_2O)_{n+1}{}^*$$

$$H^+(H_2O)_{n+1}{}^* + A \rightleftharpoons H^+(H_2O)_{n+1} + A^*$$

decreasing n (unimolecular decay),

$$H^+(H_2O)_n + A \rightleftharpoons H^+(H_2O)_n{}^* + A$$

$$H^+(H_2O)_n{}^* \rightarrow H^+(H_2O)_{n-1} + H_2O$$

A is a third body and the asterisk indicates that a particle has sufficient energy to make it inherently unstable. While Zook and Grimsrud gave an excellent argument for cluster growth using this model, they realized that they needed another mechanism to explain the smaller-than-expected cluster ions. They proposed collisional dissociation even though they noted, similar to the results of Figures 3 and 4, that the cluster distributions were independent of the potentials applied to the focussing lenses.

Before expanding on this model, it is necessary to first note that cluster distributions can be distorted by instrumental effects in mass spectrometry. One of these is diminished ion transmission due to mass discrimination by the quadrupole filter; another is fragmentation of the cluster during its flight through the mass analyzer; and still another is fractionation of species as a result of different speed ratios perpendicular to the expanding jet.[44] The first two favor enhanced yields for lower molecular weight clusters, while the latter favors the sampling of higher molecular

weight clusters. In modern quadrupole mass spectrometers, adjustments can be and are made to minimize the effects of mass discrimination. On the EXTREL C50 mass spectrometer, this is accomplished using the "resolution" and "ΔM" controls. The cluster fragmentation and species fractionation processes, however, are beyond simple adjustments. Their effects can only be minimized by carefully selecting the original design used to construct the mass spectrometer.

To the extent that instrumental effects do not effect cluster distributions, gas dynamic mechanisms can be used to explain the results of Table 4. The most obvious feature for a gas expansion under isentropic conditions is that gas density and translational temperature decrease (except for local regions of supersaturation) with increasing distance from the nozzle.[44] In the continuum flow regime where equilibrium conditions are collisionally maintained, this means that ion cluster distributions are adjusting to decreasing water concentrations until the distribution is "frozen" by a lack of collisions. This "frozen" state will contain "smaller-than-expected" ion clusters if water concentrations in the source are used for calculations. Competing with this apparent desolvation mechanism is cluster growth precipitated by the reduced temperature created by the expansion. In terms of Buckle's model, this arises from the intermediate ion, $H^+(H_2O)_{n+1}*$, having a lower internal energy and having a longer lifetime within which it can be stabilized by collision with a neutral gas molecule.[26] Both processes depend upon the buffer gas used for the expansion. Heavier buffer gases will lead to slower expansions and lighter buffer gases will lead to faster expansions. There are more opportunities for the development of distortions in slow expansions than in faster expansions because more collisions are possible and the terminal translational temperature is higher. For faster expansions, reduced residence times may also minimize the effects expected for lower temperature. Consequently, Zook and Grimsrud found cluster distributions equivalent to equilibrium conditions when using a helium buffer gas.

CONCLUSIONS

Mass spectrometry is an invaluable tool in characterizing the ion composition of ion mobility peaks in ion mobility spectrometry. When the ion composition is found to be a mixture of ion clusters, the observed cluster distribution may not be an accurate representation of the ion clusters in the IMS. Depending on the buffer gas, lower clusters can form by equilibrating with reduced concentrations in the continuum regime of the expansion and larger clusters can form by collisional stabilization in the cooled jet stream. Besides water, nitrogen molecules can also add to the ion clusters created in ion mobility spectrometry. Even though nitrogen is non-polar, this addition is made possible by an ion-induced dipole interaction between the ion and molecule.

REFERENCES

1. Griffin, G.W., Dzidic, I., Carroll, D.I., Stillwell, R.N. and Horning, E.C. Ion Mass Assignments Based on Mobility Measurements: Validity of Plasma Chromatographic Mass Mobility Correlations. *Anal. Chem.*, **45**, 1204-1209 (1973).

2. Lin, S.N., Griffin, G.W., Horning, E.C. and Wentworth, W.E. Dependence of Polyatomic Ion Mobilities on Ionic Size. *J. Chem. Phys.*, **60**, 4994-4999 (1974).

3. Wessel, M.D. and Jurs, P.C. Prediction of Reduced Ion Mobility Constants from Structural Information Using Multiple Linear Regression Analysis and Computational Neural Networks. *Anal. Chem.* **66**, 2480-2487 (1994).

4. Revercomb, H.E. and Mason, E.A. Theory of Plasma Chromatography/Gaseous Electrophoresis - A Review. *Anal. Chem.* **47**, 970-983 (1975).

5. Mason, E.A. Ion Mobility: Its Role in Plasma Chromatography. In Plasma Chromatography, Carr, T.W., Ed. Plenum, NY, 1984, chapt. 2.

6. Spangler, G.E. and Lawless, P.A. Ionization of Nitrotoluene Compounds in Negative Ion Plasma Chromatography. *Anal. Chem.* **50**, 884-892 (1978).

7. Hagen, D.F. Characterization of Isomeric Compounds by Gas and Plasma Chromatography. *Anal. Chem.* **51**, 870-874 (1979).

8. Karpas, Z., Stimac, R.M. and Rappoport, Z. Differentiating Between Large Isomers and Derivation of Structural Information by Ion Mobility Spectrometry Mass-Spectrometry Techniques. *Int. J. Mass Spectrom. Ion Processes* **83**, 163-175, (1988).

9. Karpas, Z. Ion Mobility Spectrometry of Aliphatic and Aromatic Amines. *Anal. Chem.* **61**, 684-689 (1989).

10. Karpas, Z. The Structure and Mobility in Air of Protonated Ketones. *Int. J. Mass Spectrom. Ion Processes* **107**, 435-440 (1991).

11. Karpas, Z. and Pollevoy, Y. Ion Mobility Spectrometric Studies of Organophosphorus Compounds. *Anal. Chim. Acta* **259**, 333-338 (1992).

12. Karasek, F.W., Kim, S.H. and Rokushika, S. Plasma Chromatography of Alkyl Amines. *Anal. Chem.* **50**, 2013-2016 (1978).

13. McKeown, M. and Siegel, M.W. Atmospheric Pressure Ionization for Mass Spectrometry. *Amer. Lab.* **7**(11), 89-99 (1975).

14. Carroll, D.I., Dzidic, I., Horning, E.C. and Stillwell, R.N. Atmospheric Pressure Ionization Mass Spectrometry. *Appl. Spectros. Rev.* **17**, 337-406 (1981).

15. Preston, J.M. and Rajadhyax, L. Effect of Ion/Molecule Reactions on Ion Mobilities. *Anal. Chem.* **60**, 31-34 (1988).

16. Ashkenas, H. and Sherman, F.S. Experimental Methods in Rarefied Gas Dynamics. In Rarified Gas Dynamics, 4th Symposium, Vol. II, DeLeeuw, J.H., Ed. Academic Press, NY, 1966, p. 84.

17. Fite, W.L. Expansion of Gases from Molecular Beam Sources. Research Note #1, Extranuclear Laboratories, Inc., Pittsburgh, PA, 1971.

18. Fricke, J., Jackson, W.M. and Fite, W.L. Mass and Phase Spectrometry of a Water Vapor Jet. *J. Chem. Phys.* **57**, 580-582 (1972).

19. Mitchum, R.K. and Korfmacher, W.A. Atmospheric Pressure Ionization Mass Spectrometry. *Anal. Chem.* **55**, 1485A-1499A (1983).

20. Anderson, J.B. and Fenn, J.B. Velocity Distributions in Molecular Beams from Nozzle Sources. *Phys. Fluids* **8**, 780-787 (1965).

21. Miller, D.R. Free Jet Sources. In <u>Atomic and Molecular Beam Methods</u>, G. Scoles, Ed. Oxford Univ. Press, Oxford, England, 1988, chapt. 2.

22. Douglas, D.J. and French, J.B. Gas Dynamics of the Inductively Coupled Plasma Mass Spectrometry Interface. *J. Anal. At. Spectrom.* **3**, 743-747 (1988).

23. Searcy, J.Q. and Fenn, J.B. Clustering of Water on Hydrated Protons in a Supersonic Free Jet Expansion. *J. Chem. Phys.* **61**, 5282-5288 (1974).

24. Searcy, J.Q. A Kinetic Model for Clustering of Water on Hydrated Protons in a Supersonic Free Jet Expansion. *J. Chem. Phys.* **63**, 4114-4119 (1975).

25. Carlon, H.R. and Harden, C.S. Mass Spectrometry of Ion Induced Water Clusters: An Explanation of the Infrared Continuum Absorption. *Appl. Opt.* **19**, 1776-1786 (1980).

26. Zook, D.R. and Grimsrud, E.P. Measurement of Ion Clustering Equilibria of Proton Hydrates by Atmospheric Pressure Ionization Mass Spectrometry. *J. Phys. Chem.* **92**, 6374-6379 (1988).

27. Kambara, H. and Kanomata, I. Ionization Characteristics of Atmospheric Pressure Ionization by Corona Discharge. *Mass Spectrom.* **24**, 229-236 (1976).

28. Kambara, H. and Kanomata, I. Determination of Impurities in Gases by Atmospheric Pressure Ionization Mass Spectrometry. *Anal. Chem.* **49**, 270-275 (1977).

29. Kambara, H., Mitsui, Y. and Kanomata, I. Identification of Clusters Produced in an Atmospheric Pressure Ionization Process by a Collisional Dissociation Method. *Anal. Chem.* **51**, 1447-1452 (1979).

30. Spangler, G.E. and Carrico, J.P. Membrane Inlet for Ion Mobility Spectrometry (Plasma Chromatography). *Int. J. Mass Spectrom. Ion Phys.* **52**, 267-287 (1983).

31. Extrel Corporation, 240 Alpha Drive, Box 11512, Pittsburgh, PA 15238.

32. Spangler, G.E. Membrane Interface for Ion Mobility Detector Cells. U.S. Patent 4,311,699, The Bendix Corporation, Southfield, MI, January 1982.

33. New England Nuclear, 549 Albany Street, Boston, MA 02118.

34. Matheson Gas Products, 30 Seaview Dr., P.O. Box 1587, Secaucus, NJ 07096.

35. Balston, Inc., 260 Neck Rd., Haverhill, MA 01835.

36. W.R. Grace & Co., Davison Chemical Division, P.O. Box 2117, Baltimore, MD 21203.

37. Ametek, 455 Corporate Blvd., Pencador Corporate Ctr., Newark, DE 19702.

38. <u>CRC Handbook of Chemistry and Physics</u>, R.C. Weast, Ed. CRC Press, Boca Raton, FL, 1983.

39. Amirav, A., Even, U. and Jortner, J. Cooling of Large and Heavy Molecules in Seeded Supersonic Beams. *Chem. Phys.* **51**, 31-42 (1980).

40. Hayes, J.M. Analytical Spectroscopy in Supersonic Jets. *Chem. Rev.* **87**, 745-760 (1987).

41. Noggle, J.H. Physical Chemistry. Little, Brown and Company, Boston, MA, 1985.

42. Ashkenas, H. and Sherman, F.S. Experimental Methods in Rarefied Gas Dynamics. In Rarefied Gas Dynamics, 4th Symposium, Vol. II, J.H. de Leeuw, Ed. Academic Press, NY, 1966, pp. 89-91.

43. Buckle, R.E. A Kinetic Theory of Cluster Formation in the Condensation of Gases. *Trans. Faraday Soc.* **65**, 1267-1288 (1969).

44. Kappes, M. and Leutwyler, S. Molecular Beams of Clusters. In Atomic and Molecular Beam Methods, Vol. 1, G. Scoles, Ed. Oxford University Press, Oxford, 1988, chapt. 15.
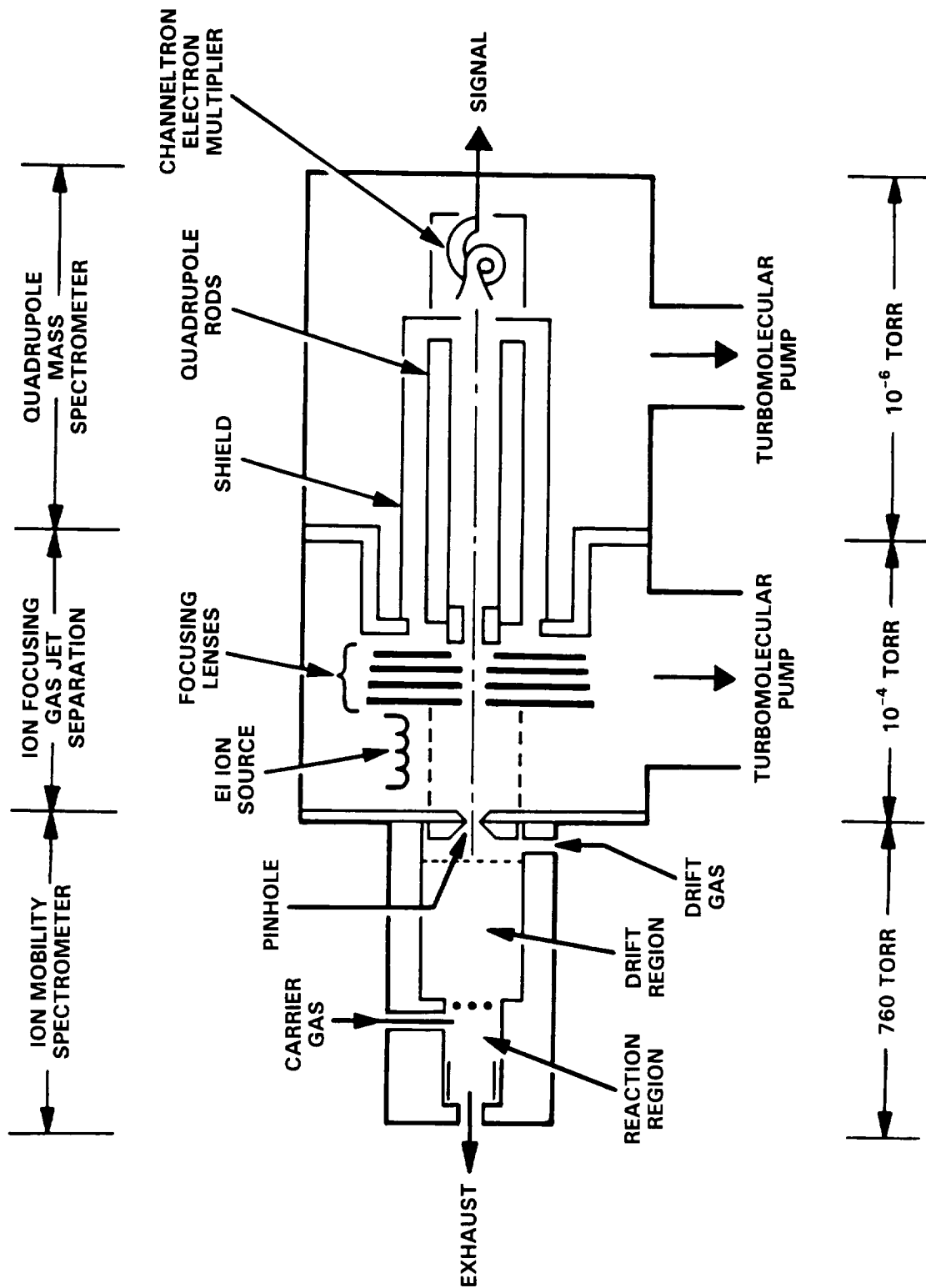
Figure 1. Functional Diagram for the Ion Mobility Spectrometer/Mass Spectrometer System.

127

PINHOLE

VACUUM
FLANGE

WIRE
BASKET

FOCUSING
LENSES

LENS 1

LENS 2

LENS 3

LENS 4

LENS 5

TO QUADRUPOLE
MASS SPECTROMETER
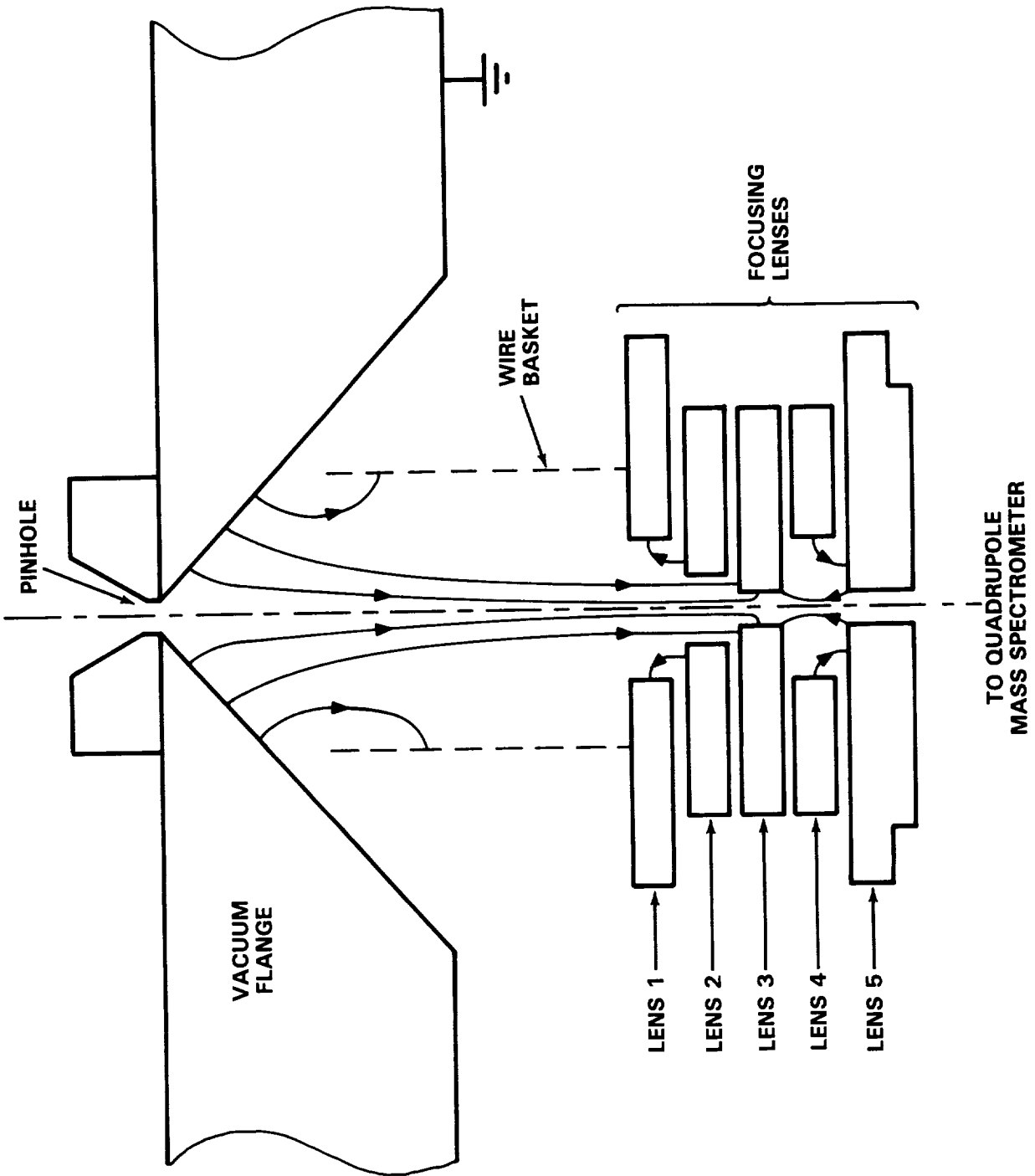
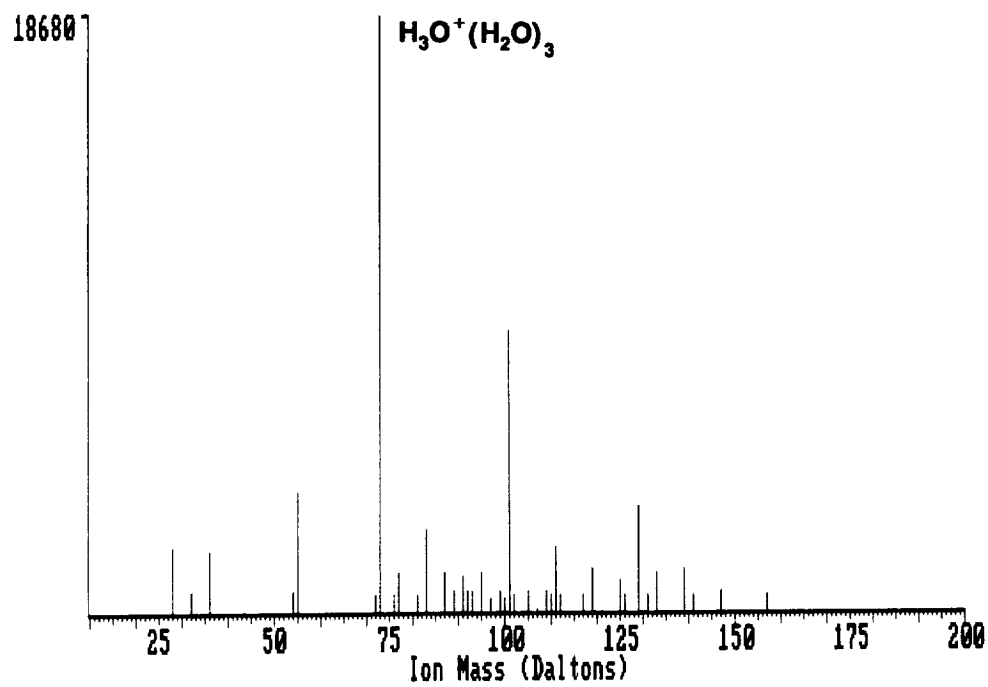Figure 2. Expanded Sketch for the Pinhole Ion Sampler and Mass Spectrometer Focussing Lens Assembly.

128
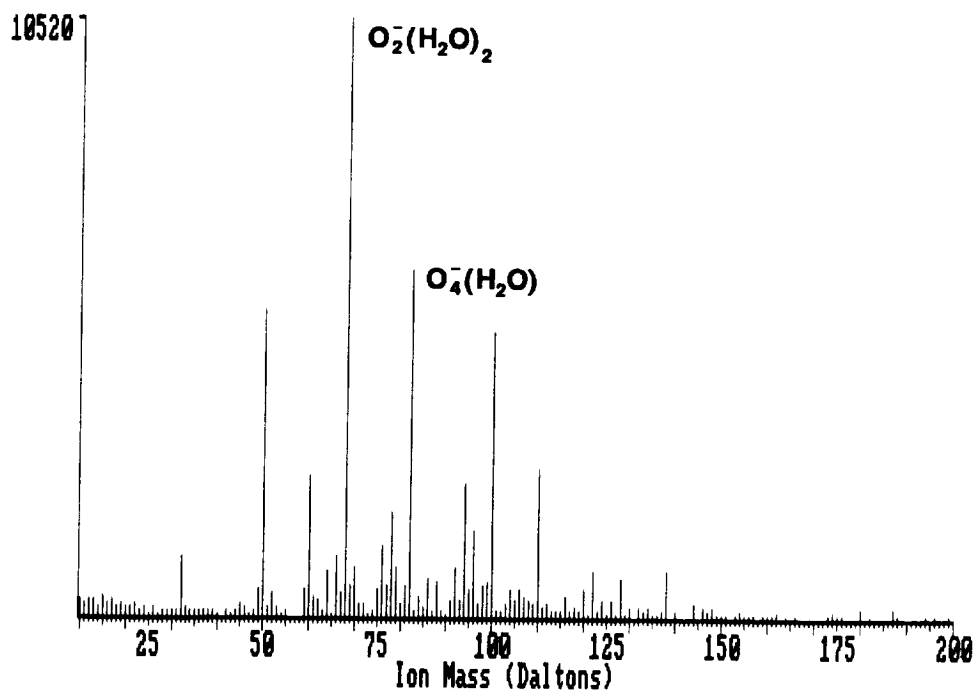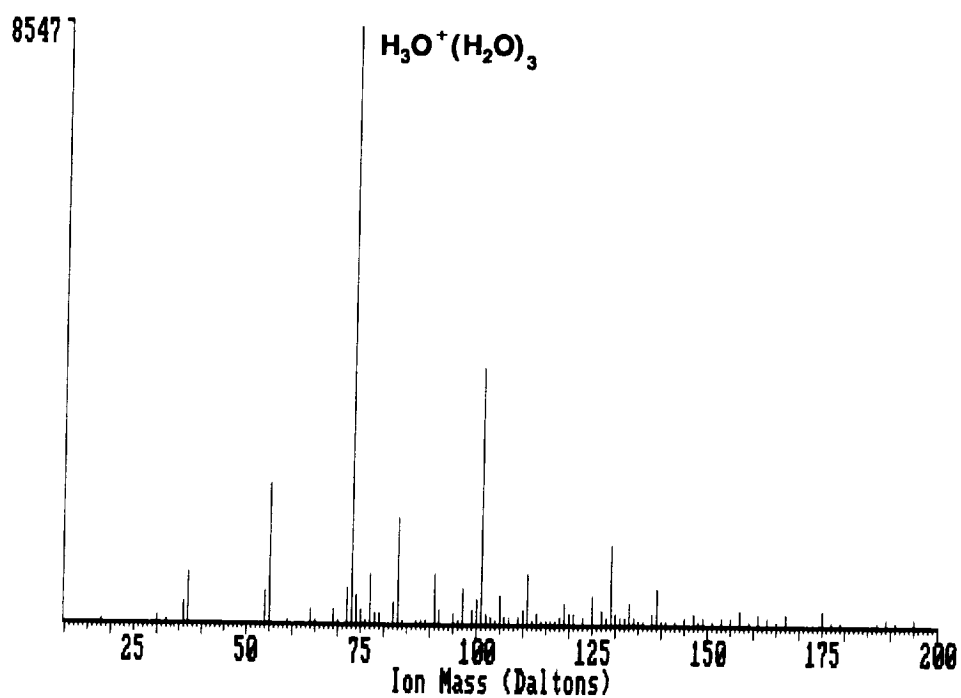
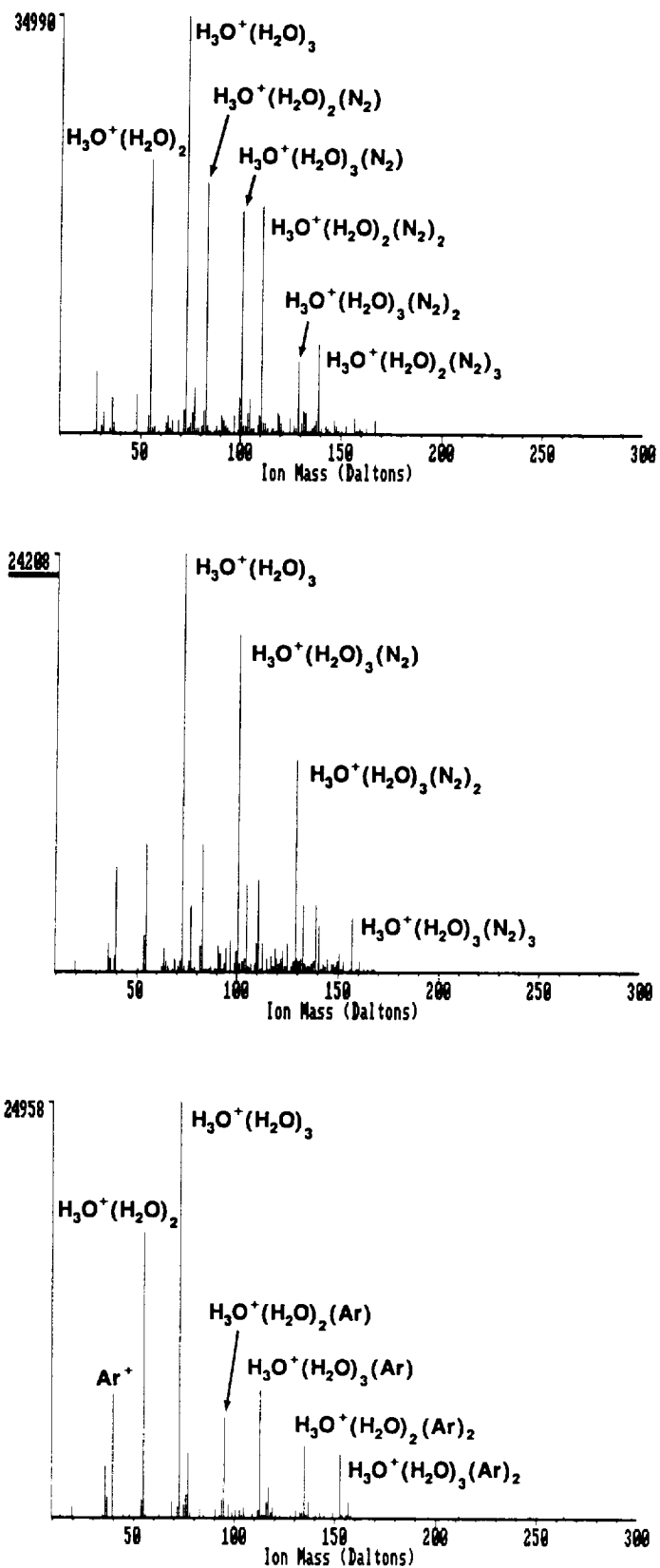**Figure 3. Positive (top) and Negative (bottom) Reactant Ions Using the Lower Voltages for the Ion Focussing** Lens Assembly.
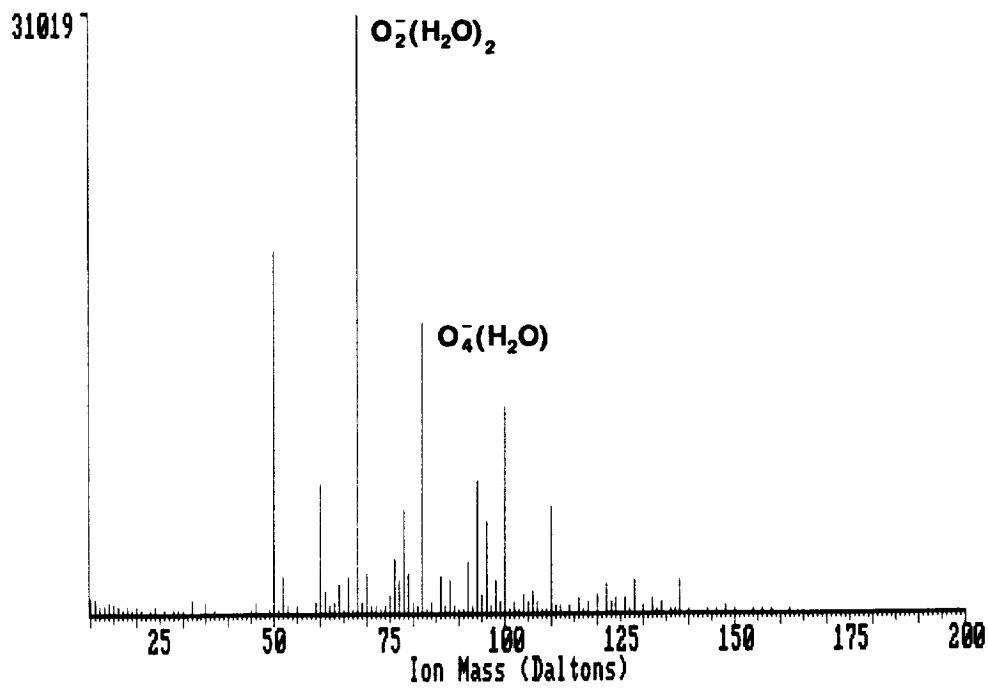
Figure 4. Positive (top) and Negative (bottom) Reactant Ions Using the Higher Voltages for the Ion Focussing Lens Assembly.

Figure 5. Positive Reactant Ions Using Purified Air for the Carrier, Drift and Sample Gases (top); Argon for the Carrier, Drift and Sample Gases (bottom); and Purified Air for the Carrier and Sample Gases and Argon for the Drift Gas (middle).
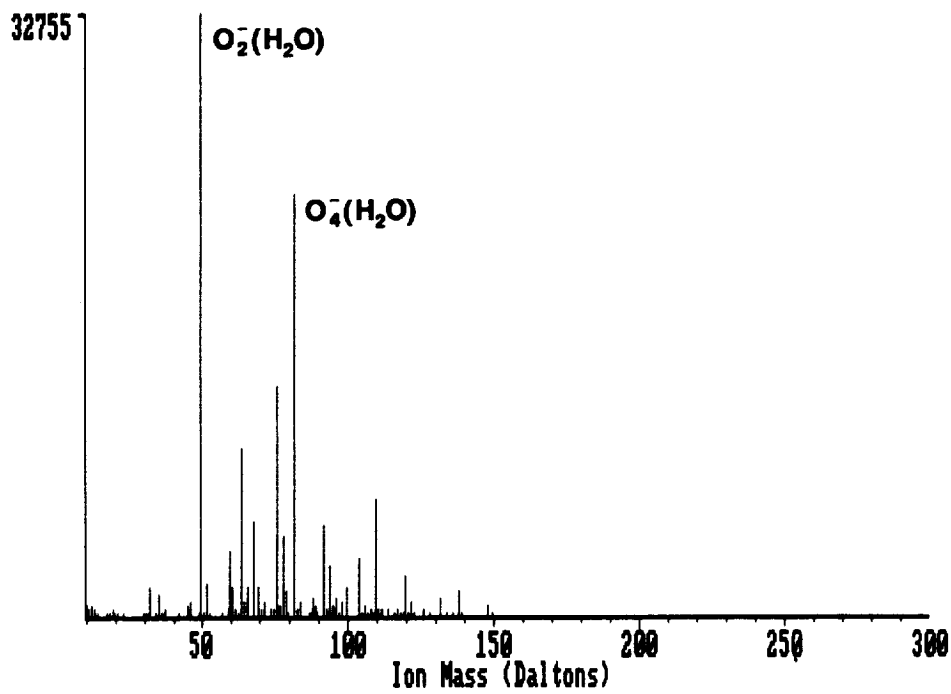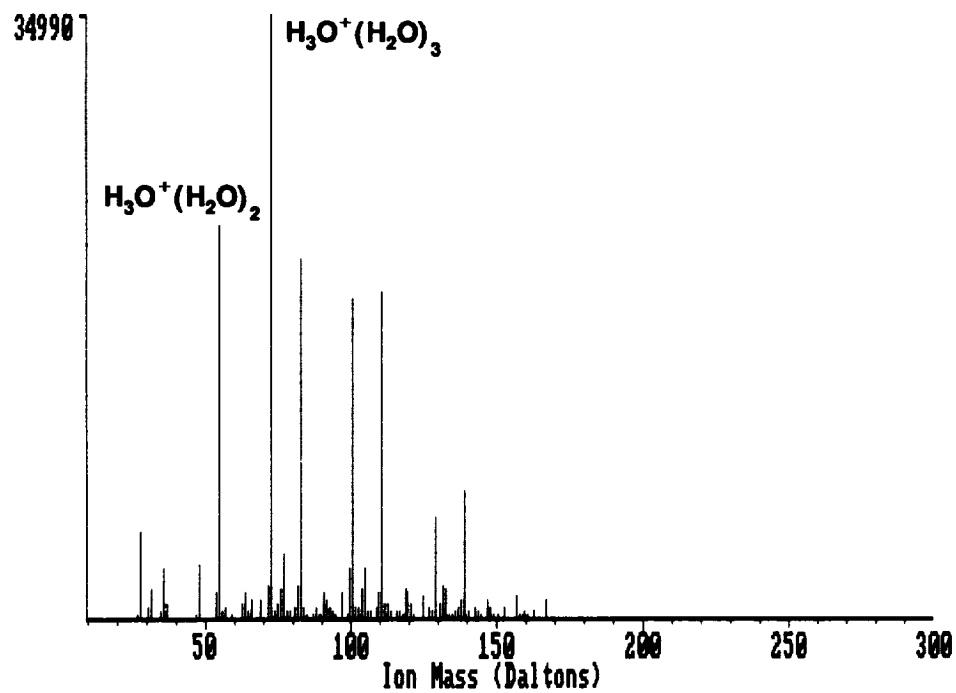
131

Figure 6. Positive (top) and Negative (bottom) Reactant Ions Before 13 ppm Water Introduced into the IMS.
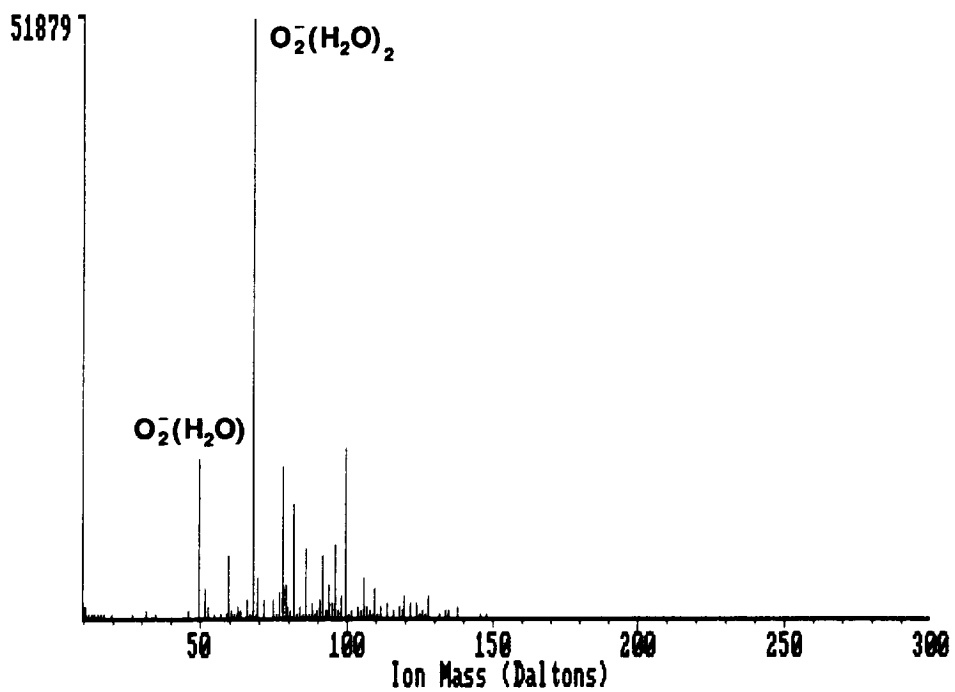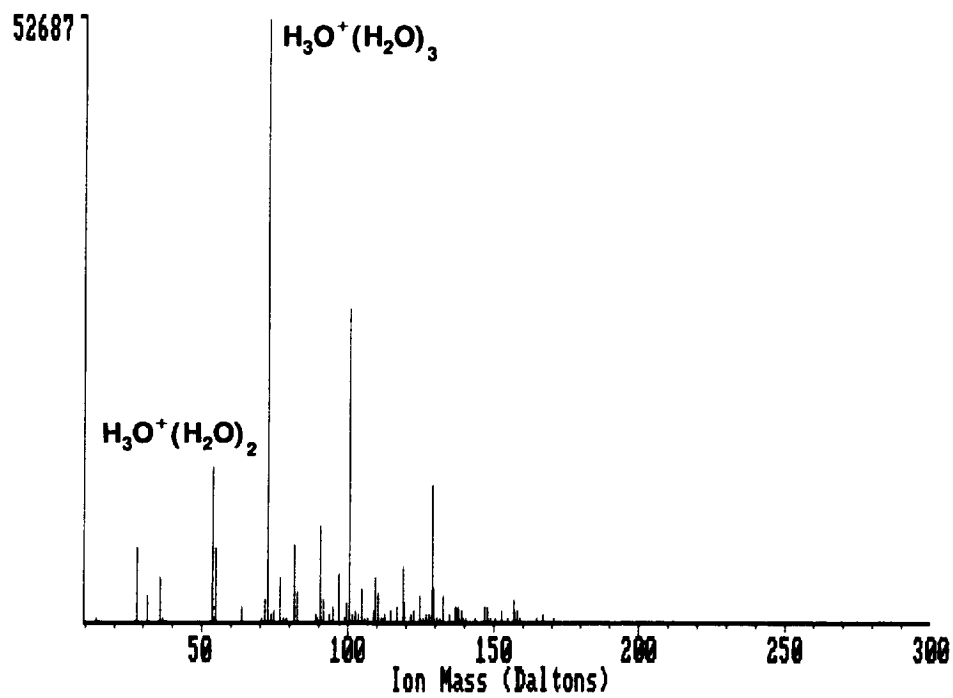
Figure 7: Positive (top) and Negative (bottom) Reactant Ions After 13 ppm Water Introduced into the IMS.